Adsorption (2014) 20:829–842
DOI 10.1007/s10450-014-9625-9

Interactions of thiophenes with C300 Basolite MOF in solution by the temperature-programmed adsorption and desorption, spectroscopy and simulations

Muslum Demir · Michael L. McKee · Alexander Samokhvalov

Received: 26 March 2014 / Revised: 21 June 2014 / Accepted: 23 June 2014 / Published online: 5 July 2014

Abstract Aromatic sulfur compounds, e.g. thiophene (T), benzothiophene (BT), dibenzothiophene (DBT), 4,6-dimethyldibenzothiophene (4,6-DMDBT) are present in petroleum and fossil fuels, and cause air pollution, degradation of catalytic converters, deactivation of fuel-reforming catalysts. In this paper, we report kinetic, thermodynamic, spectroscopic and computational studies of adsorption of T, BT, DBT, and 4,6-DMDBT from solution in *n*-alkane on metal–organic framework (MOF) Basolite C300 at 25–115 °C. The novel temperature-programmed adsorption/desorption method allows the in situ measurement of an adsorption capacity at the variable temperature, and after the cycle "adsorption/desorption". Adsorption of BT, DBT and 4,6-DMDBT at 25 °C occurs via the formation of the stoichiometric 1:1 adsorption complexes. BT adsorbs reversibly, while 4,6-DMDBT adsorbs irreversibly. The formation of the adsorption complex of the aromatic sulfur compound with MOF is confirmed by the fluorescence spectroscopy for the first time. The DFT computations of the geometry and energy of dispersive versus electronic interactions of T and DBT with the structural units of the C300 MOF are reported for the first time. The mechanism of adsorption is proposed as a combination of dispersive and electronic interactions of the aromatic sulfur compounds with BTC linker and Cu(II) CUS of C300 MOF.

M. Demir · A. Samokhvalov (✉)
Department of Chemistry, Rutgers University, 315 Penn St., Camden, NJ 08102, USA
e-mail: alexsam@camden.rutgers.edu

M. L. McKee
Department of Chemistry and Biochemistry, Auburn University, Auburn, AL 36849, USA

Keywords Metal–organic frameworks · Thiophenes · Adsorption · Desorption · Temperature-programmed · Fluorescence · Density functional theory

1 Introduction

Aromatic sulfur compounds such as thiophenes, benzothiophenes, dibenzothiophenes (Fig. 1) are abundantly present in virtually all fossils and liquid fossil fuels: petroleum, shale oil, the U.S. tar sands, Canadian bitumen, gasoline, diesel, jet and heating fuels, and the streams of petroleum refineries. After an enforcement of the Ultra Low Sulfur (ULS) U.S. gasoline (30 ppmw total sulfur) and diesel (15 ppmw total sulfur) standard, certain commercial liquid fuels still contain the high concentrations of the aromatic sulfur compounds. The U.S. military liquid logistic fuels contain up to 5,000 ppmw total sulfur (Samokhvalov 2012), and commercial U.S. heating oils up to 10,000 ppmw (Samokhvalov 2012) (with sulfur present as the large-ring aromatic sulfur compounds). The industrial catalytic hydrodesulfurization (HDS) is not very effective (Song 2002) for the selective removal of the large-ring substituted aromatic sulfur compounds. Mechanistic studies of reactive adsorption, i.e. an adsorption with chemical destruction of the adsorbate molecule and with the formation of the molecular products of reaction, e.g. (Ryzhikov et al. 2008) and of the non-reactive adsorption of aromatic sulfur compounds from liquid phase, e.g. (Samokhvalov et al. 2010) have been conducted and reviewed (Samokhvalov and Tatarchuk 2010); the non-reactive adsorption is promising for commercialization (Jayaraman et al. 2008).

Metal–organic frameworks (MOFs) constitute the new class of advanced metal–organic polymers with very high

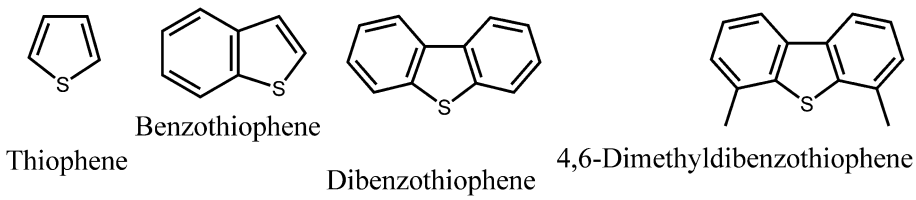

Fig. 1 Molecular structure of aromatic sulfur compounds

surface area and pore volume. An ability of the MOFs to selectively absorb gases e.g. hydrogen (Saha et al. 2009), acetylene (Xiang et al. 2011), carbon dioxide (Keskin et al. 2010) was studied extensively. The MOFs feature a moderate to high stability toward oxygen and temperature, but often undergo hydrolysis e.g. (Bezverkhyy et al. 2014). Thus, an adsorption on the MOFs could be utilized for the adsorption/desorption processes in the non-aqueous liquid phase, at both an ambient and elevated temperatures. However, an adsorption on the MOFs in the liquid phase was studied much less compared to adsorption in the gas phase. One of the most widely studied MOFs is HKUST-1 aka $Cu_3(BTC)_2$, where BTC is benzene-1,3,5-tricarboxylate linker unit. HKUST-1 contains the "paddlewheel" Cu_2O_8 dimers with open Cu(II) coordinatively unsaturated sites (CUS). C300 Basolite MOF from Sigma-Aldrich has the same empirical Hill formula $C_{18}H_6Cu_3O_{12}$ as HKUST-1. C300 MOF is structurally similar (Gimeno-Fabra et al. 2012) to HKUST-1 as judged by the BET total surface area S(BET), total pore volume V_p determined at 0.95 P/P_o, and the micropore volume V_m determined by the t-plot analysis by Harkins and Jura. Specifically, the S(BET) is 1,950 m^2/g for HKUST-1 and 1,694 m^2/g for C300, the Vp is 0.80 cm^3/g for HKUST-1 and 0.72 cm^3/g for C300, and the V_m is 0.77 cm^3/g for HKUST-1 and 0.70 cm^3/g for C300 MOF.

The solvent in the model fuels studied for an adsorptive desulfurization with the MOFs is usually isooctane (Blanco-Brieva et al. 2011) with boiling point 99 °C that models gasoline with a high octane number and a low boiling point range. On the other hand, model diesel, heating oils and refinery oils should have a long straight chain alkane with a high cetane number and a high boiling point as solvent. However, only one paper (Achmann et al. 2010) reports an adsorption of the aromatic sulfur compound (thiophene) from alkane with a long straight chain, *n*-dodecane on the MOF. One should note that thiophene with boiling temperature 84 °C is not abundantly present in the typical refinery streams that contain *n*-dodecane with boiling temperature 214–218 °C. Adsorption on the MOFs from the model fuels where both aromatic sulfur compound and alkane solvent have the low boiling temperatures (typical model gasoline) or both have the high boiling temperatures (typical model diesel or refinery oil) has not been studied, to our knowledge.

For gaseous adsorbates, the formation of the stoichiometric 1:1 adsorption complexes was reported for acetylene, ethylene and propylene on only one MOF, Fe_2(dobdc) (Bloch et al. 2012). The term "stoichiometric adsorption complex" means that one gas molecule is adsorbed per one Fe(II) CUS in the MOF. On the other hand, the adsorption capacities of the MOFs in the liquid phase are usually reported in the units of g sulfur/kg sorbent or mmol sulfur/g sorbent (Liu et al. 2012) rather than on molar base, so it is not known whether the adsorption complexes with a distinct chemical stoichiometry are formed. Further, although the formation of the adsorption complexes in the system "liquid/solid" is usually assumed, their direct spectroscopic characterization is very seldom as recently noted by us (Samokhvalov and Tatarchuk 2010). One can mention the solid state NMR characterization of DBT adsorbed from the model fuel on Ag+/SBA-15 and Ag+/SiO_2 sorbents (McKinley and Angelici 2003). Fluorescence is a convenient non-destructive spectroscopic method (Samokhvalov and Tatarchuk 2010), however there is only one paper on the characterization of the adsorption complexes of aromatic compounds in the system "liquid/solid" by the fluorescence spectroscopy (Shan et al. 2004). The spectroscopic characterization of the adsorption complexes of the aromatic sulfur compounds by the fluorescence spectroscopy was not reported, to our knowledge.

Density functional theory (DFT) is an ab initio quantum chemical technique that is a standard method of calculations of the energy and geometry of surface sites and reaction pathways in adsorption and surface chemical reactions. The structure of several MOFs including HKUST-1 has been determined by the density-functional based tight-binding (DFTB) method (Lukose et al. 2012; Farrusseng et al. 2009). The DFT calculations of an interaction of ethylene and ethane with a Cu–tricarboxylate complex (the structural unit of HKUST-1) were reported (Nicholson and Bhatia 2006). Calculations of heats of adsorption of Kr, Xe, N_2, CO_2, CH_4, *n*-C_4H_{10}, and *i*-C_4H_{10} on HKUST-1 were also reported (Farrusseng et al. 2009). The quantum chemical calculations of the structure of adsorption complexes of HKUST-1 with CO were recently published (Petkov et al. 2012). Adsorption of aromatic compound aniline on several MOFs was studied by computational screening (Xiao et al. 2013). To our knowledge, no reports are available on quantum chemical computations

of the energy of dispersive versus electronic interactions of any MOF with aromatic sulfur compounds.

Recently, we reported the structural properties and oxidation and coordination states of Cu(II) adsorption site in the Cu–ZnO/SiO_2 desulfurization sorbents (Dhage et al. 2010). We also reported the molecular structure and thermal stability of adsorption complexes formed by thiophene and DBT with the family of Ag–TiO_2 desulfurization sorbents (Samokhvalov et al. 2010a, b, c, d). Most recently, we reported a combined experimental and DFT computational study of reactive adsorption of hydrogen sulfide onto Cu(II) sites in Cu–ZnO/SiO_2 desulfurization sorbents (Dhage et al. 2013).

Herein, we report for the first time the thermodynamic, spectroscopic and computational studies of adsorption of T, BT, DBT, and 4,6-DMDBT on Basolite C300 MOF from the long-chain alkane n-$C_{14}H_{30}$ as solvent at the variable temperature as measured in situ. First, we utilize the new method of the in situ temperature-programmed adsorption/desorption (TPAD), where desorption is non-destructive, it proceeds back to the liquid phase without the contact of the sample with air, and an adsorption capacity can be measured in situ again after the cycle "adsorption/desorption". Second, we report for the first time the formation of the 1:1 stoichiometric adsorption complexes of BT, DBT and 4,6-DMDBT with C300 MOF. Third, we report for the first time a direct spectroscopic proof of the formation of the adsorption complex of DBT with C300 MOF using the wavelength-dependent fluorescence spectroscopy. Fourth, we report for the first time the DFT calculations of geometry of adsorption complexes of thiophene and DBT with major structural units of this MOF, and the contributions from both dispersive and electronic interactions to the energy of bonding.

2 Experimental

2.1 Chemicals

Thiophene (T), benzothiophene (BT), dibenzothiophene (DBT), 4,6-dimethyl dibenzothiophene (4,6-DMDBT) (Fig. 1), n-tetradecane, n-octane and C300 Basolite MOF were purchased from Sigma Aldrich.

2.2 Model fuels

Model fuels were 0.033 M solutions of T, BT, DBT, and 0.022 M solution of 4,6-DMDBT in n-tetradecane; molar concentrations were chosen to be below the solubility limits of the respective aromatic sulfur compound. Model fuels were prepared by the sonication of the calculated amount of the given aromatic sulfur compound in neat n-tetradecane at room temperature until complete dissolution.

2.3 Activation of C300 prior to adsorption

C300 Basolite was activated at 150 °C and $<1 \times 10^{-4}$ Torr for 24 h before the adsorption. Care was taken to protect an activated C300 from moisture in ambient air, thus the activated C300 was immediately placed into an adsorption vial filled with the chosen model liquid fuel.

2.4 Kinetics of adsorption

A sample of 0.300 g activated C300 was mixed with 50 ml of model fuel, placed in a sealed adsorption vial that was attached to mechanical shaker, and held at constant temperature and continuous shaking for up to 24 h. The content of each adsorption vial was protected from ambient air with the septum made of corrosion-resistant silicon rubber. An aliquot of 0.2 ml was periodically collected by the syringe through the septum, centrifuged and analyzed by the HPLC–UV and UV–Vis absorption spectroscopy to determine chemical composition of the liquid phase.

2.5 The in situ temperature-programmed adsorption/desorption (TPAD)

Activated C300 MOF (0.300 g) was mixed with 50 ml model fuel, and placed into adsorption vial equipped with silicone stopper and septum. The vial was held under continuous shaking for the duration of the whole TPAD experiment. The temperature was held at 25 °C for 12 h until the equilibrium (based on the kinetics of adsorption determined as above), and a small aliquot (0.1 ml) was collected, centrifuged, analyzed by the HPLC–UV and UV–Vis spectroscopy. Then, the temperature was linearly increased (at a constant rate) to 75 °C for 1.5 h using the proportional integral derivative (PID) temperature controller (SYL-2342P, Auber Instruments), the mixture was allowed to re-equilibrate for 10 h, and sampling with chemical analysis was repeated. Then, the temperature was raised to 115 °C, held constant for 10 h, and sampling with chemical analysis was conducted. Finally, the adsorption vial was linearly cooled to 25 °C, allowed to equilibrate for 10 h, and sampling with chemical analysis was conducted again.

2.6 Chemical analysis of model fuels

For the qualitative analysis, the HPLC–UV instrument model Gold (from Beckman Coulter) with Model 168 UV–Vis detector and reversed phase C18 5-μm column was used. The eluent was 25 % vol. water/75 % vol. acetonitrile as reported elsewhere (Robertson and Bandosz 2006). For the quantitative analysis, we used the UV/VIS spectrometer Cary 50 from Biorad in absorption mode. The clear supernatant from the sampled aliquot (0.1 ml) was

volumetrically diluted with pure n-$C_{14}H_{30}$ by factor 100, and quartz microcuvette with optical path $l = 0.3$ cm or 0.1 cm was used to construct calibration plots. Optical absorption at the spectral maxima was used: 325 nm for DBT and 4,6-DMDBT, 299 nm for BT, and 250 nm for T. The UV–Vis calibration plots are linear for all compounds studied, and molar concentrations were determined by the standard Bougert–Lambert–Beer method.

2.7 Fluorescence spectroscopy

The 1.5 cc quartz fluorescence cuvette was filled with solid DBT, closed with the PTFE stopper, DBT was melted just above melting temperature (97–100 °C) by briefly heating the cuvette in the oven, and allowed to solidify at 25 °C. The sample of adsorption complex of DBT with activated C300 MOF was obtained by adding melted DBT to the activated C300 MOF in the fluorescence quartz cuvette under dry argon, to achieve molar ratio DBT/C300 MOF = 12 (using the nominal molecular mass of C300 MOF at 605 a.m.u.). The suspension of melted DBT and C300 was promptly mixed while DBT was still in a liquid form, and was allowed to solidify at 25 °C; the resultant sample has a uniform visual appearance. The fluorescence spectroscopy measurements were conducted using Cary Eclipse fluorescence spectrometer. The angular accessory (from Agilent Inc.) for strongly absorbing solid samples was used to minimize spectral distortions due to both primary and secondary re-absorption (Lakowicz 2006) of light. Wavelength of the fluorescence excitation λ_{exc} was 280, 290, 300 or 310 nm. The width of the excitation and emission slits was the same, and was chosen based on the intensity of the fluorescence.

2.8 Quantum chemical calculations

Quantum chemical calculations were performed using Gaussian 09 program and full geometry optimization using B3LYP/SDD in DFT. We used DFT-D3 to compute the dispersion correction (Grimme et al. 2011) to the binding energy of thiophene and DBT to the Cu_6O_{12} unit of HKUST-1. The solvation free energy for thiophene and DBT in n-hexadecane was calculated at the SMD/B3LYP/6-311+g(d,p) level (Marenich et al. 2009).

3 Results and discussion

3.1 Optical absorption of solutions of aromatic sulfur compounds

Figure 1 shows molecular structures of the studied thiophenes. Molar concentration of T, BT, DBT in model fuel

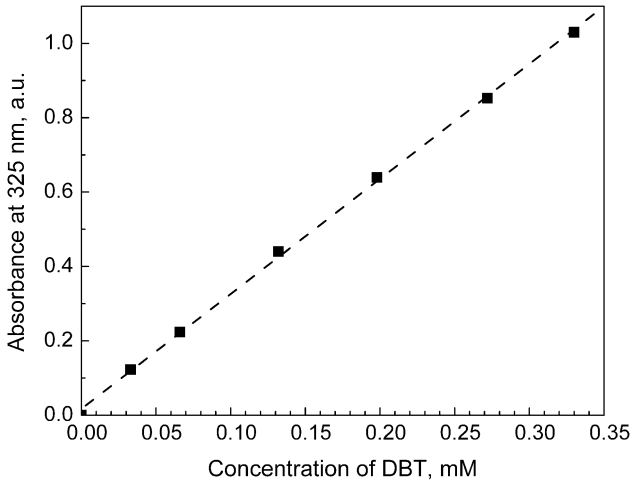

Fig. 2 Calibration plot of the UV–Vis absorption spectroscopy to determine the molar concentration of DBT

at 0.033 M corresponds to the total content of sulfur at 1,400 ppmw that is representative of heating oils, military and civil jet fuels (Samokhvalov 2012), streams of petroleum refining such as heavy vacuum oils and naphthas of fluid catalytic cracking (FCC) that are the largest source of organic sulfur compounds in commercial gasoline (Ito and vanVeen 2006). Absorption spectra of model fuels containing thiophene, BT, DBT and 4,6-DMDBT are consistent with published data. Specifically, the model fuel DBT in n-$C_{14}H_{30}$ has absorption peaks at 235 nm (the β band), at 285 nm (the p band), and at 325 nm (the α band) (Jacob 1990) corresponding to the $2A_1$ electronic term (Spanget-Larsen and Thulstrup 2003). Figure 2 shows a calibration curve of a quantitative determination of molar concentration of DBT, [DBT] in the model fuel with n-$C_{14}H_{30}$ as solvent using the UV–Vis absorption spectroscopy (diluted sample, absorbance measured at 325 nm). Calibration curves are linear within the range of the concentrations used by us.

4 The in situ temperature-programmed adsorption/desorption (TPAD)

In the reported adsorption studies, in the "spent" C300 MOF sorbent after adsorption of DBT from isooctane (Blanco-Brieva et al. 2011), an oxidized form S(VI) was found by the XPS, thus one cannot expect to re-use a regenerated C300 for adsorption, since DBT sulfone is not soluble in hydrocarbons. However, prior to the XPS the sample was handled in air (Blanco-Brieva et al. 2011), so an oxidation of the adsorption complex might have taken place before the XPS, and XPS spectroscopy itself can be destructive to the specimen and can lead to errors in

determining an oxidation state (Suezer 2000). Therefore, it would be useful to study adsorption so that (1) desorption is non-destructive to both the sorbent and adsorbate, (2) desorption proceeds back to the liquid phase without the contact of the sample with ambient air, and (3) adsorption capacity can be measured again in situ after the cycle "adsorption/desorption". To our knowledge, such adsorptive desulfurization with MOFs was never reported. Thus, we decided to measure the adsorption capacity of C300 MOF towards several aromatic sulfur compounds after an adsorption and the subsequent in situ temperature-induced desorption, with the sample always protected from air, using the novel in situ TPAD method (Fig. 3). C300 Basolite MOF is thermally stable up to 327 °C in the absence of water (Gimeno-Fabra et al. 2012), so we decided to test an adsorption of the aromatic sulfur compounds from solution in n-$C_{14}H_{30}$ on C300 MOF at 25–115 °C.

In the reported (Achmann et al. 2010) adsorption of thiophene from dodecane on Cu-BTC MOF under the standard conditions, an equilibrium is achieved in less than 1 h. We have determined the kinetics of adsorption of DBT from the model fuel on C300 MOF at 25 °C and 1 atm; after less than 5 h, the [DBT] remains constant within an error 5 %; an adsorption of T shows the similar kinetics. For both diffusion-limited and reaction-limited kinetics of adsorption, the rate of adsorption is higher when the temperature is higher. Figure 3 shows the typical temperature–time (T–t) profile of the in situ TPAD method used by us; for each temperature setpoint at 25, 75 and 115 °C, the time to reach an adsorption equilibrium at that temperature is chosen to be 10 h.

Figure 4a shows the changes in molar concentration of BT, [BT] in the model fuel during the in situ TPAD experiment. After adsorption at 25 °C, [BT] decreases until molar ratio (adsorbed BT)/(Cu_2O_8 units in C300 MOF) = 0.98. After an increase of temperature to 115 °C, a nearly complete desorption of BT from C300 MOF occurs. Upon the further cooling to 25 °C, the [BT] returns to approximately the same concentration as before the adsorption at 25 °C. After one cycle "adsorption/desorption", the only compound found in liquid phase is BT as determined by the HPLC–UV; therefore, adsorption of BT is non-reactive. We conclude that BT adsorbs on C300 Basolite reversibly, can be nearly completely desorbed at 115 °C and re-adsorbed at 25 °C.

Figure 4b shows the change in molar concentration of DBT in model fuel, [DBT] during the in situ TPAD. After an adsorption at 25 °C, [DBT] decreases until molar ratio (adsorbed DBT)/(Cu_2O_8 units in C300 MOF) = 0.92. After an increase of the temperature to 75 °C and equilibration, [DBT] increases, and it further increases at 115 °C indicating a partial desorption of DBT from the MOF to the fuel. This is different from the case of BT where at 115 °C, a nearly complete desorption occurs. In the model fuel with DBT after the TPAD cycle "adsorption/desorption" at 25–115 °C, the only compound found by the HPLC–UV is DBT; therefore, adsorption of DBT is non-reactive. DBT cannot be completely desorbed from C300 MOF at the temperature up to 115 °C. The [4,6-DMDBT] decreases after adsorption at 25 °C until molar ratio (adsorbed 4,6-

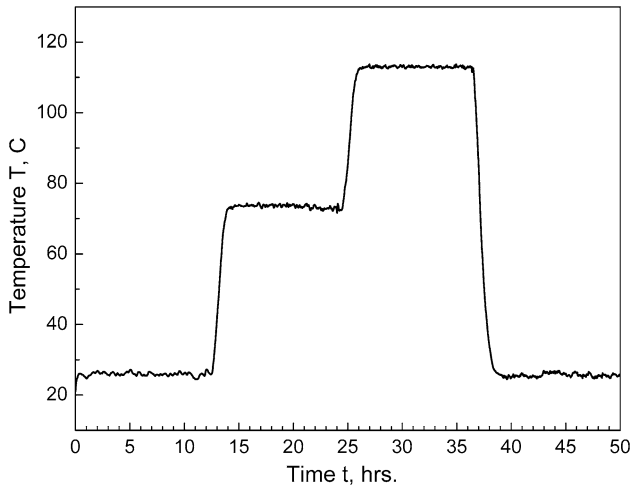

Fig. 3 The typical in situ temperature-programmed adsorption/desorption (TPAD) profile temperature–adsorption time (T–t)

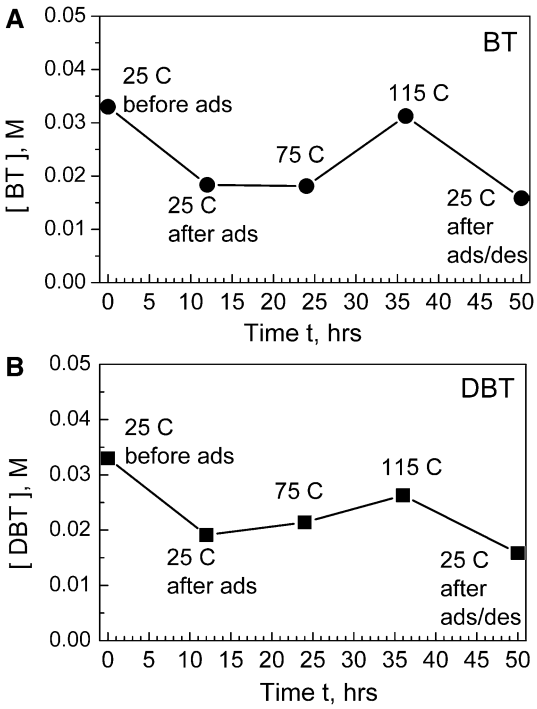

Fig. 4 The changes in the molar concentration of aromatic sulfur compounds in liquid phase during an adsorption/desorption on C300 MOF in n-tetradecane by the in situ TPAD at 25–115 °C: **a** BT; **b** DBT

DMDBT)/(Cu_2O_8 units in Cu300 MOF) = 1.02, and further remains constant up to 115 °C, and is constant after the subsequent cooling to 25 °C (TPAD data not shown, see Table 1). In the model fuel with 4,6-DMDBT after the TPAD cycle "adsorption/desorption" at 25–115 °C, the only compound in liquid phase found by the HPLC–UV is 4,6-DMDBT. We conclude that 4,6-DMDBT strongly adsorbs to C300 via a non-reactive adsorption and cannot be desorbed up to 115 °C. The reported findings can be used for the development of the method of selective separation of aromatic sulfur compounds from their mixed solutions in aliphatic hydrocarbons by the difference in their molecular size: BT could be separated from 4,6-DMDBT at elevated temperatures.

Figure 5 shows the adsorption capacities of BT, DBT and 4,6-DMDBT on C300 MOF from *n*-tetradecane at 25, 75, 115 °C and again at 25 °C as determined by us using the in situ TPAD method. Adsorption capacity of thiophene at 75 and 115 °C cannot be reliably determined by the in situ TPAD method, due to partial evaporation of thiophene from the model fuel (boiling point of thiophene is 84 °C). We note that the fused-ring aromatic sulfur compounds have rather high boiling points; for example, BT has boiling point at 221 °C. The fused ring aromatic sulfur compounds are concentrated in kerosene and oil refinery fractions where the long straight-chain alkanes such as *n*-tetradecane with boiling point at 253 °C are also concentrated. Therefore, *n*-tetradecane is a suitable solvent for model diesel, refinery streams and oils. On the other hand, isooctane with its low boiling point at 99 °C is not a representative solvent for the model diesel and refinery oils. In Fig. 5, adsorption capacity at 25 °C is higher than 70 g/kg sorbent for BT, DBT and 4,6-DMDBT with *n*-tetradecane as solvent. These adsorption capacities are significantly higher than those reported for C300 MOF with isooctane as solvent, e.g. (Liu et al. 2012).

To explain the difference, we need to consider the sizes of the nanocavities in the C300 MOF and molecular size of the solvent. HKUST-1 has a trimodal pore size distribution (Senkovska et al. 2012): (1) a large cuboctahedral cage I with diameter about 13 Å that contains coordinatively unsaturated Cu(II)–Cu(II) sites, (2) a large cuboctahedral cage II with diameter 11 Å, and (3) a small octahedral cage

Table 1 The stoichiometric ratios (moles of adsorbed aromatic sulfur compound)/(moles of Cu_2O_8 units in C300 MOF)

Adsorbate	Temperature (°C)			
	25	75	115	25 (after cooling)
BT	0.98	0.99	0.12	1.14
DBT	0.92	0.78	0.44	1.14
4,6-DMDBT	1.02	1.02	1.06	1.08

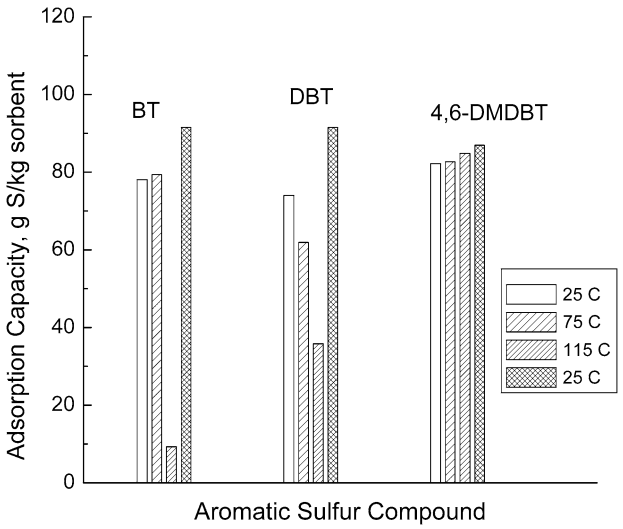

Fig. 5 Adsorption capacities (g sulfur per kg sorbent) on C300 MOF at 25–115 °C for BT, DBT and 4,6-DMDBT

with diameter 4–5 Å. The largest cage I is formed by twelve paddle-wheel units $Cu_2(COO)_4$ where Cu(II) site is pointing inside the cage, so this cage is hydrophilic. The Cu(II) is in distorted octahedral geometry, with one Cu–Cu bond and four Cu–O bonds; the sixths coordination bond is formed by Cu(II) CUS with the molecule of adsorbate, or it remains free in the "activated" form of HKUST-1 (Vitillo et al. 2008). The pores of the second and third kind are less hydrophilic, since their interior is formed by the aromatic rings of the BTC linker. We propose that the molecule of the solvent, *n*-$C_{14}H_{30}$ with the largest linear dimension of 30 Å is too large to fit within any nanocavity of C300 MOF, so it does not compete with adsorption of the molecules of aromatic sulfur compounds for adsorption sites. Therefore, aromatic sulfur compounds can have the highest possible adsorption capacity, and could form the stoichiometric adsorption complexes as further elaborated below. We further note that the adsorption capacity at 25 °C after one cycle adsorption/desorption during the in situ TPAD (Fig. 5) is not smaller than that at 25 °C before adsorption. Therefore, no decomposition of the C300 MOF occurred during the TPAD at 25–115 °C for >40 h. On the other hand, there is a small increase of adsorption capacity of BT, DBT and 4,6-DMDBT at 25 °C after the in situ TPAD that can be explained by an additional in situ thermal activation of C300 MOF due to heating during the TPAD experiment.

We further note that in the majority of studies, adsorption capacity of aromatic sulfur compounds was expressed in mass units, and in only one study it was also expressed in mmol/kg sorbent (Liu et al. 2012). Table 1 summarizes the molar stoichiometric ratios in the adsorption complexes of aromatic sulfur compounds as determined by us from the

respective in situ TPAD experiments. Molar ratios are expressed as (moles of adsorbed aromatic sulfur compound) per (moles of the Cu_2O_8 units in C300 MOF).

Molar ratios close to unity indicate the formation of the 1:1 stoichiometric adsorption complexes where the molecule of adsorbate, e.g. DBT is attached in the direct vicinity of the "paddlewheel" Cu_2O_8 unit in C300 MOF. Our data indicate that one molecule of BT, DBT or 4,6-DMDBT coordinates, on average, to one Cu(II) in C300 MOF at 25 °C. To learn further about adsorption mode of aromatic sulfur compounds on C300 MOF, one needs to use the spectroscopic and computational methods (below).

5 Fluorescence spectra of aromatic sulfur compound DBT and C300 MOF

One method of preparation of the sample for the fluorescence spectroscopy would be an adsorption of aromatic sulfur compound on C300 MOF from the model fuel with the subsequent evaporation of an alkane solvent. However, the obtained powdered sample (typical particle size of C300 MOF 16 μm as in the specs by the manufacturer) strongly scatters the UV light in the fluorescence experiment. In addition, a constant packing density (mg per cm^3 of cuvette volume) is not possible to achieve with powdered samples. Therefore, we prepared the solid samples for the fluorescence spectroscopy at room temperature (Fig. 6) similarly to the reported method of sample preparation for the fluorescence spectroscopy in cryogenic matrix (Del Riccio et al. 2000), see Experimental. Since melting temperature of DBT is 97–100 °C, such temperature during the sample preparation mimics the interaction of DBT with C300 MOF at the highest temperature of the TPAD (Fig. 3) at 115 °C with the subsequent cooling to the lowest temperature of the TPAD at 25 °C.

Figure 6a shows the fluorescence spectrum of pure DBT ($\lambda_{exc} = 310$ nm). A broad fluorescence band is resolved into several vibronic subbands that were fitted by the multiple Gaussian function. Specifically, the first subband centered at 340 nm with the Full Width at the Half Maximum (FWHM) of 8 nm is assigned to the 0–0 component of the $S_1 \rightarrow S_0$ fluorescence transition in solid DBT, based on the reported 0–0 fluorescence band of solid DBT (Bree and Zwarich 1971) at 29,923 cm^{-1} at 4 K; the difference in the spectral position is due to the higher measurement temperature in our experiments. The second subband at 356 nm with the FWHM = 15 nm is assigned to the fluorescence $S_1 \rightarrow S_0$ transition coupled with the in-plane vibrations of aromatic ring of DBT (Bree and Zwarich 1971) at 1,310 or 1,610 cm^{-1}. The third subband at 371 nm with the FWHM = 10 nm is assigned to the fluorescence $S_1 \rightarrow S_0$ transition coupled with both 1,310 and 1,610 cm^{-1} in-plane vibrations of DBT molecule (Bree and Zwarich 1971). The broad subband at 381 nm with the FWHM = 23 nm cannot be reliably assigned based on the available literature, and likely represents the fluorescence background. Thus, in pure DBT, the 0–0 transition is rather weak (Fig. 6a) as compared to vibronic subbands that is consistent with the reported small quantum yield of fluorescence of DBT at the 0–0 transition (Alvarez-Valtierra et al. 2009). We have used $\lambda_{exc} = 310$ nm rather than $\lambda_{exc} = 325$ nm that corresponds to absorption maximum of DBT in alkane solution or vapor phase (Spanget-Larsen and Thulstrup 2003), in order to resolve both fluorescence spectrum and the Raleigh photoexcitation line.

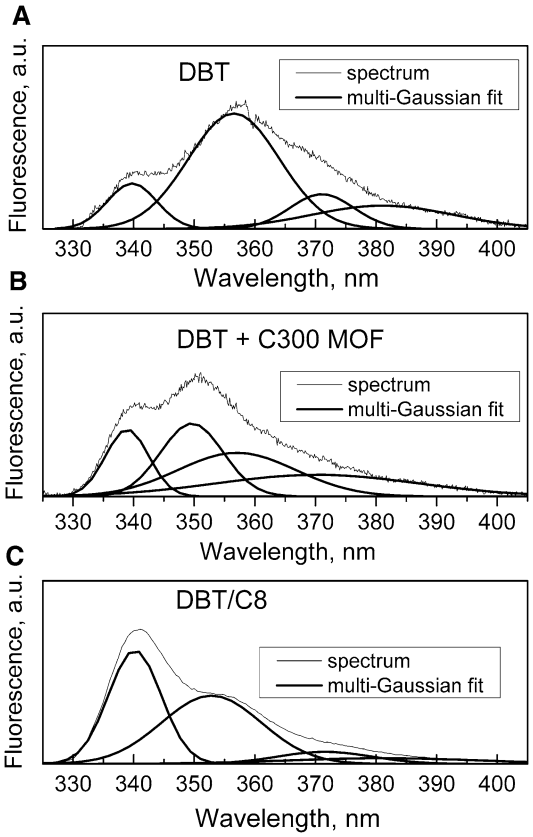

Fig. 6 The fluorescence spectra at $\lambda_{exc} = 310$ nm: **a** pure DBT, **b** adsorption complex of DBT with C300 MOF, and **c** 0.033 M solution of DBT in *n*-octane. *Solid thin lines* fluorescence spectra; *solid thick lines* fitting with the multi-Gaussian function

In the UV–Vis Diffuse Reflectance spectrum of activated HKUST-1, there is a broad band with an edge at about 330 nm due to a ligand to metal charge transfer (LMCT) transition from oxygen to Cu(II) ions (Prestipino et al. 2006). In was found by us that C300 MOF does not show any fluorescence spectrum within 280–800 nm range with λ_{exc} varied from 260 to 320 nm, when measured in the mixture with solid alkane *n*-$C_{20}H_{42}$ as matrix. Therefore,

C300 MOF has no fluorescence in the UV–Vis range, so any fluorescence from the mixture of C300 and DBT would be from the "free" DBT or DBT in adsorption complex with the MOF. It was not possible to prepare the samples with the 1:1 molar ratio DBT/Cu_2O_8 paddlewheel unit in C300 MOF by our method. Figure 6b shows the fluorescence spectrum of the mixture of DBT and C300 MOF with molar ratio DBT/C300 = 12. With such a molar ratio and Hill formula $Cu_3C_{18}H_6O_{12}$ for C300 MOF, as many as eight molecules of DBT are present per each Cu_2O_8 "paddlewheel" unit of the C300 MOF, so our samples for fluorescence spectroscopy contain an excess of DBT versus the 1:1 stoichiometry.

In Fig. 6b, the following changes versus fluorescence spectrum of pure DBT (Fig. 6a) can be noted. First, the 0–0 transition is centered at the same wavelength 338 nm that implies rather weak electronic interaction of the DBT molecule with adsorption sites of C300 MOF that is consistent with the in situ TPAD of DBT on C300 MOF (Fig. 4b), with partial desorption of DBT at 115 °C. It is also known that the secondary absorption artifact in the fluorescence spectra caused by the strongly absorbing component of the sample would cause red shift in the fluorescence spectrum (Burdett et al. 2010). Therefore, the absence of the red shift of the 0–0 transition of the DBT molecule in the fluorescence spectrum of the mixture DBT + C300 MOF (Fig. 6b) versus that in pure DBT (Fig. 6a) indicates that the secondary absorption due to C300 MOF is not present in our spectra, as expected when using the angle accessory in the fluorescence experiment (see Experimental). Second, the first vibronic subband at 349 nm (Fig. 6b) is blue-shifted from 356 nm in pure DBT (Fig. 6a). This indicates the change in the energy of quantum oscillator of adsorbed DBT due to its molecular environment after adsorption. Third, the 0–1 vibronic subband of DBT in the spectrum of adsorption complex at 349 nm (Fig. 6b) is just ca. 20 % higher than the 0–0 transition, while the 0–1 vibronic subband of pure DBT at 356 nm (Fig. 6a) is more than twice higher than the respective 0–0 fluorescence transition. This finding also indicates the significant changes in molecular environment of adsorbed DBT that affect its fluorescence coupled vibrations. The UV–Vis DRS spectrum of HKUST-1 is continuous in the near UV spectral range of interest (Prestipino et al. 2006) and has no absorption peaks with the comparable FWHM that would modulate the fluorescence from DBT due to secondary absorption. Therefore, the subbands in the fluorescence spectra in Fig. 6 are not affected by the secondary absorption of fluorescence originating from the DBT by the C300 as noted by us above, thus they represent the changes in the spectrum of DBT due to a different molecular environment of the DBT in the adsorption complex with C300 MOF versus that of pure DBT.

Figure 6c shows the fluorescence spectrum of the 0.033 M solution of DBT in *n*-octane. The *n*-octane solvent has no fluorescence peaks as was checked in the reference experiment. The spectrum was fitted with the four-Gaussian function. First, spectral positions of the 0–0 transition are about the same for neat DBT (Fig. 6a), DBT + C300 MOF (Fig. 6b) and DBT in solution (Fig. 6c) that is consistent with the weak electronic interactions of DBT molecules with molecular environment in all cases. Second, the relative intensity of the 0–0 vibronic component in the fluorescence spectrum (at ca. 340 nm) versus the 0–1 transition (at ca. 355 nm) is significantly different for DBT in solution and in neat DBT. We calculated the ratio of the areas A of the fitted vibronic components, A(0–0)/A(0–1) in the fluorescence spectra. For neat DBT (Fig. 6a), this ratio A(0–0)/A(0–1) = 0.22, while for the solution of DBT (Fig. 6c), this ratio A(0–0)/A(0–1) = 0.88. In neat DBT, each molecule of DBT is surrounded with molecules of DBT only. On the other hand, in the 0.033 M solution of DBT in *n*-octane, one DBT molecule is surrounded, on average, with 187 molecules of *n*-octane solvent. Therefore, the isolated DBT molecules in solution cause the high ratio A(0–0)/A(0–1) in the fluorescence spectrum. For the mixture of DBT and C300 MOF (Fig. 6b), the ratio A(0–0)/A(0–1) = 0.65 that is an intermediate value between those for the solution of DBT (Fig. 6c) and neat DBT (Fig. 6a). Therefore, in the mixture of DBT with C300 MOF (Fig. 6b), there is a significant amount of DBT molecules in an isolated state due to their quantum confinement in the nanocavity of the C300 MOF. The difference in the ratio A(0–0)/A(0–1) for isolated molecules of DBT in the mixture with MOF (Fig. 6b) and DBT in solution (Fig. 6c) is apparently due to the presence of an excess DBT molecules in the solid sample. Still, the ratio A(0–0)/A(0–1) = 0.65 for the mixture of DBT and C300 MOF is closer to the ratio A(0–0)/A(0–1) = 0.88 for the isolated DBT molecules in solution, than to the ratio A(0–0)/A(0–1) = 0.22 for the neat solid DBT where the DBT molecules interact with each other. In our recent paper (Dai et al. 2014), we have investigated the vibronic structure in the fluorescence spectra of the naphthalene molecules in the stoichiometric adsorption complex formed by naphthalene with F300 MOF that has the same BTC linker as C300 MOF. In the stoichiometric adsorption complex of naphthalene with activated F300 MOF, quantum confinement of the adsorbed naphthalene molecule was found based on the close similarity between the fluorescence spectrum of naphthalene in the adsorption complex and naphthalene in liquid solution (Dai et al.2014). Thus, the fluorescence spectra in Fig. 6 provide an indication that adsorbed DBT molecules preferentially interact with functional groups within the nanocavity of the MOF.

Third, the 0–1 vibronic component in the spectrum of adsorption complex (Fig. 6b) is blue-shifted versus its position in both neat DBT and DBT in solution. This indicates an oscillator coupling of adsorbed DBT molecule with the neighboring functional groups of the C300 MOF that are different from the molecular environment of the emitting DBT molecule in neat DBT (DBT molecules) and DBT in solution (*n*-octane molecules). Quantum confinement of an aromatic adsorbate has been demonstrated by the change in the fluorescence spectrum of pure naphthalene versus naphthalene adsorbed within the nanopores of cellulose sorbent (Tozuka et al. 2002). We interpret the change of the relative intensity of vibronically coupled 0–1 transition of DBT versus the 0–0 transition (Fig. 6a) upon the formation of adsorption complex with C300 MOF (Fig. 6b) as a result of quantum confinement of DBT molecule within the nanocavity of C300 MOF.

Figure 7a shows the fluorescence spectrum of pure DBT obtained at various photoexcitation wavelengths $\lambda_{exc} = 280$, 290, and 300 nm. One can see that the spectral shape is about the same for all λ_{exc} studied and is similar to that in Fig. 6a. This is consistent with the reported strong Herzberg-Teller coupling of the S_1 excited state with the higher S_2 state (Alvarez-Valtierra et al. 2009), so the observed fluorescence spectrum (Fig. 7a) originates from the $S_1 \rightarrow S_0$ transition in the DBT molecule, even with DBT molecule excited off-resonance. Figure 7b shows the fluorescence spectrum of the mixture of DBT and C300 MOF with molar ratio DBT/C300 = 12 at $\lambda_{exc} = 280$, 290, and 300 nm. Again, the spectral shape is about the same for all λ_{exc} studied and is similar to that in Fig. 6b. Therefore, spectral differences between the neat DBT and its mixture with C300 MOF that contains the adsorption complex are confirmed by the wavelength-dependent fluorescence spectroscopy.

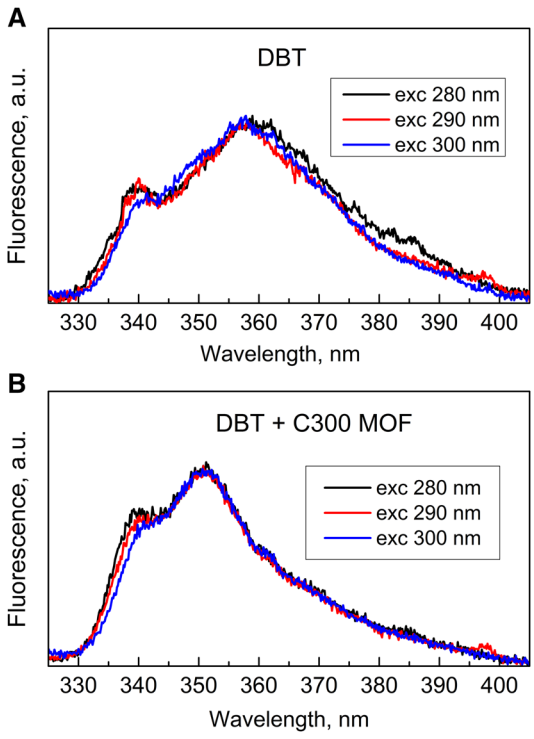

Fig. 7 The wavelength-dependent fluorescence spectra at $\lambda_{exc} = 280$, 290, and 300 nm for **a** pure DBT, and **b** and adsorption complex of DBT with C300 MOF

Our findings above represent the first direct spectroscopic evidence by the fluorescence spectroscopy of the changes in electronic and vibrational states of aromatic sulfur adsorbate in the nanocavity of the MOF sorbent. We can make two conclusions from our fluorescence spectra. First, the fluorescence spectra indicate that the molecule of DBT is quantum confined within the nanocavity of the C300 MOF sorbent upon adsorption by the C300 MOF and formation of the adsorption complex. Second, vibrations of the adsorbed quantum confined DBT molecule in the adsorption complex with C300 MOF are affected by the interactions with the BTC linker and/or Cu(II) CUS. In order to learn about molecular interactions of aromatic sulfur adsorbate with C300 MOF in more detail, we conducted quantum chemical DFT simulations.

6 The DFT computations of geometry of adsorption complexes of aromatic sulfur compounds with C300 MOF

In the DFT calculations, we start with the choice of the suitable cluster of HKUST-1 MOF to model adsorption of aromatic sulfur compounds. The "large unit" $Cu_{24}O_{48}$ of HKUST-1 is too large to be studied by the DFT using reliable basis sets. Therefore, we calculated the trimer Cu_6O_{12} and tetramer Cu_8O_{16} units (only oxygen atoms inside the nanocavity counted, Fig. 8) with a full geometry optimization using B3LYP/SDD in DFT. We used the C_{3v} symmetry group for Cu_6O_{12} and C_{4v} for Cu_8O_{16}. Both Cu_6O_{12} and Cu_8O_{16} fragments maintained the curvature of the full structural unit of HKUST-1. The tetramer unit has four Cu_2O_8 paddlewheel units that comprise the hydrophilic large cavity (cuboctahedral cage I) in HKUST-1. It is known that in $Cu_3(BTC)_2$ MOF, the pairs of Cu(II) in the paddlewheel structural unit Cu_2O_4 create an antiferromagnetic (S = 0) ground spin state at cryo-temperatures, and the thermally excited S = 1 state above 80 K as found by Electron Spin Resonance (ESR) spectroscopy (Jee et al. 2010). Therefore, we calculated energies of structural units Cu_6O_{12} and Cu_8O_{16} of HKUST-1 as zero spin, low spin and high spin states (Table 2).

Table 2 shows the energy separation in different multiplicities along with expected and calculated spin-squared

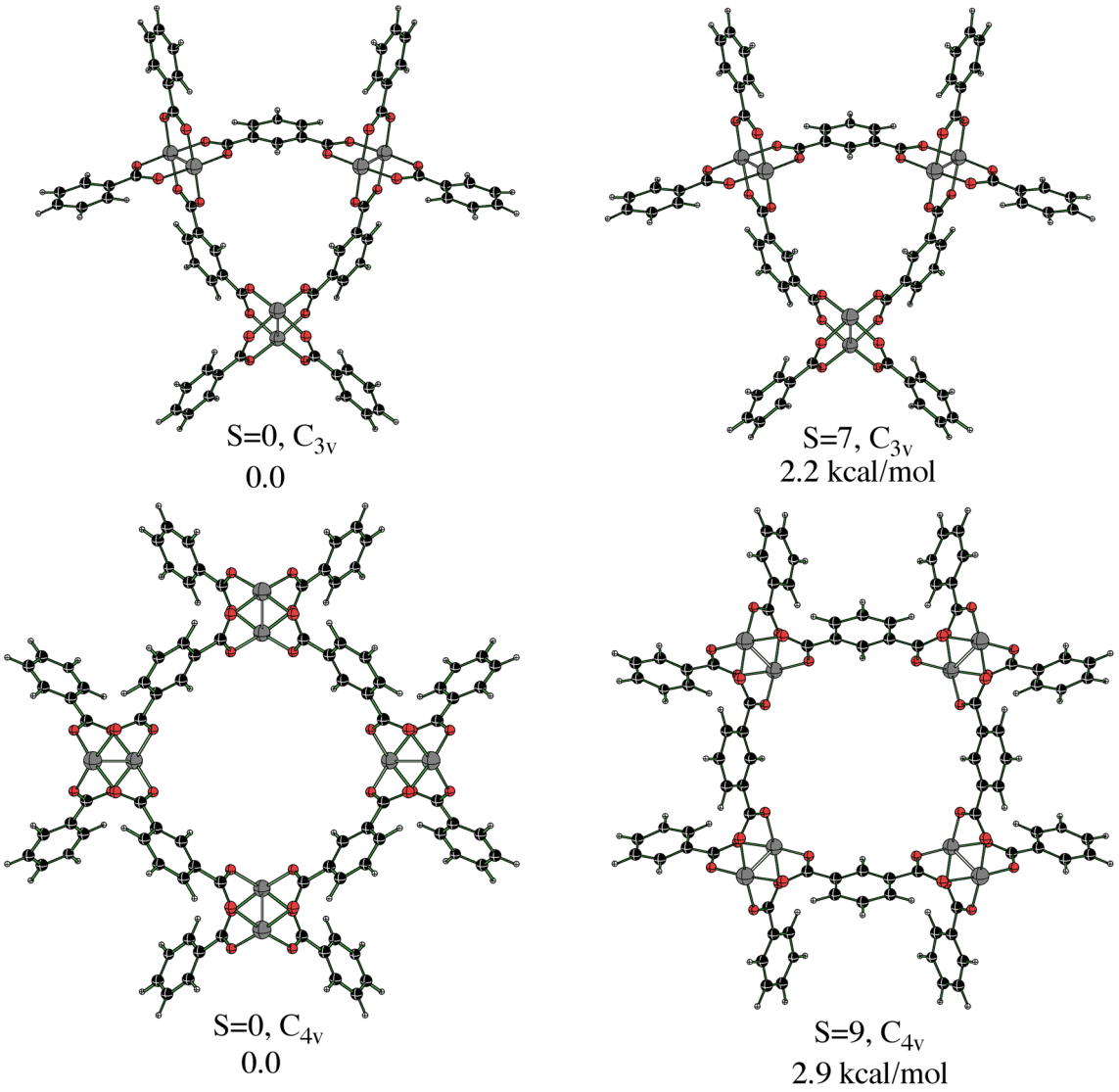

Fig. 8 Major building units of HKUST-1 calculated by DFT: Cu_6O_{12} in zero-spin and high spin state (*top row*) and Cu_8O_{16} in zero-spin and high spin state (*bottom row*). Large *grey* atoms: Cu; *red* atoms: O; *black* atoms: C; small *white* atoms: H (Color figure online)

Table 2 Calculated multiplet energy separations and spin-squared values S^2 (in parentheses) for Cu_6O_{12} and Cu_8O_{16} using B3LYP/SSD

Multiplicity (expected S^2)	Energy of Cu_6O_{12} in kcal/mol (calculated S^2)	Energy of Cu_8O_{16} in kcal/mol (calculated S^2)
1 (0.0)	0.0 (3.0)	0.0 (4.0)
3 (2.0)	0.7 (4.0)	0.7 (5.0)
5 (6.0)	1.7 (7.0)	1.5 (8.0)
7 (12.0)	2.2 (12.0)	2.2 (13.0)
9 (20.0)		2.9 (20.0)

values, S^2. The clusters with the multiplicity $2S + 1 = 1$ are of broken-symmetry where all of the inner Cu atoms have one spin-up electron and all of the outer Cu atoms have one spin-down electron. The broken-symmetry singlet (multiplicity $2S + 1 = 1$) and the high-spin state ($2S + 1 = 7$ for Cu_6O_{12} and $2S + 1 = 9$ for Cu_8O_{16} (Fig. 8) are found to be close in energy.

Further, we have calculated the optimized geometry and energy of adsorption of the smallest molecule of sulfur aromatic compounds (thiophene) versus the representative molecule of the large-ring aromatic sulfur compounds (DBT) on the trimer Cu_6O_{12} unit, Fig. 9. Calculation of adsorption complexes with the larger tetramer Cu_8O_{16} unit would be prohibitively long. We have optimized adsorption complexes thiophene-Cu_6O_{12} and DBT-Cu_6O_{12} as triplets ($2S + 1 = 3$). The triplet state and quintet state of complexes of Cu_6O_{12} with T and DBT were optimized at the B3LYP/SSD level. Both triplet states were lower in energy by 0.6 kcal/mol than the corresponding quintet states.

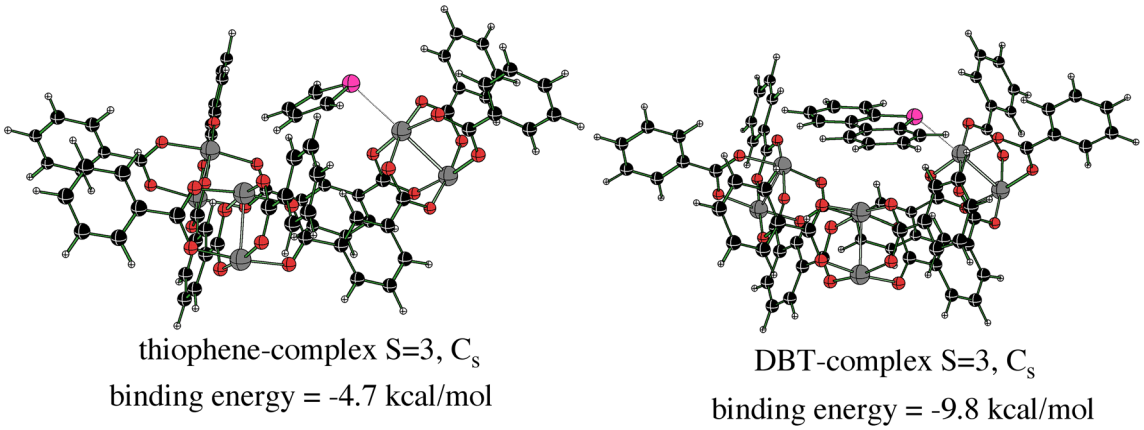

Fig. 9 Structures of adsorption complexes of Cu_6O_{12} unit with thiophene and DBT calculated by DFT. Large *pink* atom: S; large *grey* atoms: Cu; *red* atoms: O; *black* atoms: C; small *white* atoms: H (Color figure online)

The binding energy was computed for the Cu_6O_{12} + T or Cu_6O_{12} + DBT complex. Without dispersion correction and with basis set superposition error (BSSE) not included (its inclusion would decrease the binding by 2–3 kcal/mol in each case), the binding in the complex thiophene–Cu_6O_{12} is −4.7 kcal/mol, and in the complex DBT–Cu_6O_{12} it is −9.8 kcal/mol. This indicates that DBT is bound stronger than thiophene to the major structural unit of HKUST-1. We started the DFT computations with the same initial value for the Cu–S distance (3.093 A) in both adsorption complexes. Such a large bond length is within the typical range 2.412–3.286 Å for the S–Cu(II) coordination bond in the model system—coordination compounds of copper(II) with organic thiocyanates (Kabešová et al. 1995). After geometry optimization, the T and DBT interactions with the triplet Cu_6O_{12} cluster cause rather short S–Cu distances, 2.798 and 2.835 Å, respectively. At the same time, the Cu–Cu distance where the sulfur is coordinated have lengthened (2.615 Å for T–Cu_6O_{12} and 2.615 Å for DBT–Cu_6O_{12} cluster) relative to the Cu–Cu distance in the non-complexed triplet Cu_6O_{12} cluster (2.565 Å). In addition, the DBT–Cu_6O_{12} cluster has two short Cu–H interactions between a hydrogen atom on each benzene ring of DBT with different copper atoms (2.573 Å) which is consistent with agostic interactions between the DBT substrate and the Cu_6O_{12} cluster.

Further, we used DFT-D3 to compute the dispersion correction to the binding energy of thiophene and DBT to the Cu_6O_{12} cluster. The dispersion correction for binding of thiophene to Cu_6O_{12} cluster is −13.12 kcal/mol, and the correction for binding DBT to Cu_6O_{12} is −26.35 kcal/mol. We believe that the contributions from dispersive and electronic interactions to the total binding energy of adsorption of aromatic sulfur compounds on HKUST-1 or any other MOF have not been reported. Our calculated dispersion correction for adsorption of DBT of 26.35 kcal/mol can be compared with the reported adsorption energy for polyaromatic compound anthracene of about the same molecular size, taking into account that anthracene has dispersive interactions with the MOF, but contains no heteroatom. Isosteric heat of adsorption of anthracene on HKUST-1 at zero coverage is about 28 kcal/mol (Greathouse et al. 2010) that is consistent with our calculated dispersion correction for DBT at 26.35 kcal/mol. The best estimate of the total binding in our computations is the B3LYP/SDD value plus the dispersion correction, and the dispersion binding contribution is larger than the electronic part (as given by B3LYP/SDD). The binding energies of thiophene and DBT to Cu_6O_{12} and/or dispersion corrections may be computed too large, based on the typical temperatures of desorption of DBT by the in situ TPAD, Fig. 4b. The explanation is that the computations deal with the low coverages of the surface of the MOF with the adsorbate, and for the higher coverages, energy of adsorption would be lower due to the repulsions with already adsorbed molecules. To our knowledge, there are no reports on the quantification of dispersive versus electronic interactions of aromatic sulfur compounds with the MOFs. Even though the proposed quantum chemical system may not strictly quantitatively describe the TPAD data obtained with adsorption complexes of the aromatic sulfur compounds with the Cu-containing MOF on absolute basis, it will be indicative of the relative preference of binding of different molecules to the same sites in the MOFs on relative basis. A justification of scaling dispersion corrections rather than electronic interactions is that dispersion corrections are empirical values; to fit better our experimental data, we have included 50 % of total dispersion correction. With this assumption, the binding energies to the Cu_6O_{12} cluster are −11.3 and −23.0 kcal/mol for thiophene and DBT, respectively. In our experiments, we used tetradecane *n*-$C_{14}H_{30}$ as solvent for thiophene and DBT, and in

Table 3 Computed electronic energies and enthalpies at 298 K in kcal/mol

Model	Dispersive energy ΔE (kcal/mol)	−TΔS correction (kcal/mol)	Solvation free energy ΔG(sol) (kcal/mol)	Total energy (kcal/mol)
Thiophene to Cu_6O_{12}	−11.26	13.37 at 388 K	3.3	+5.4
DBT to Cu_6O_{12}	−22.98	13.37 at 388 K	8.5	−1.1
Thiophene to Cu_6O_{12}		10.28 at 298 K		+3.3
DBT to Cu_6O_{12}		10.28 at 298 K		−4.2

calculations we used *n*-hexadecane *n*-$C_{16}H_{34}$ as solvation medium. The solvation free energy for thiophene and DBT in *n*-hexadecane at the SMD/B3LYP/6-311 + g(d,p) level is −3.3 and −8.5 kcal/mol, respectively. The free energy (ΔG) of binding thiophene/DBT to Cu_6O_{12} in *n*-hexadecane (C16) is given by:

$$\Delta G = \Delta G(g) + \Delta G(\text{sol}, n\text{−C16})$$

where ΔG(sol, *n*-C16) values are −3.3 and −8.5 kcal/mol (see above).

To get ΔG(g), we need zero-point energies, heat capacity corrections and −TΔS corrections. We have computed DBT binding to one Cu_2O_8 cluster ($C_{28}H_{22}Cu_2O_9$) in the triplet state at the B3LYP/SDD level. The calculations show, not surprisingly, that the zero point and heat capacity corrections are small, but the −TΔS corrections are significant. We applied the corrections (calculated for the DBT-Cu_2O_8 complex) to the binding energies in the DBT-Cu_6O_{12} complex to estimate binding free energies, at 115 °C (388 K) and 25 °C (298 K), Table 3. Table 3 shows that the binding of thiophene to Cu_6O_{12} in *n*-hexadecane is unfavorable (nonspontaneous) at 115 and 25 °C (5.4 and 3.3 kcal/mol, respectively). The binding of DBT to Cu_6O_{12} in *n*-hexadecane is slightly favorable at 115 °C (−1.1 kcal/mol) and more favorable at 25 °C (−4.2 kcal/mol). We believe that the calculations can be used for the qualitative interpretation of adsorption of small molecules (thiophene) versus large molecules (DBT) on HKUST-1 and C300 MOF. We can make the following conclusions. First, the binding energy of DBT to Cu_6O_{12} is about twice that of thiophene. Second, the solvation free energy of DBT in *n*-hexadecane is about 5 kcal/mol larger than that of thiophene. Third, in *n*-hexadecane as solvent for adsorption, the binding of DBT to Cu_6O_{12} is stronger than the binding of thiophene to Cu_6O_{12} by about 6 kcal/mol.

Our DFT data on dispersive stabilization of adsorbed DBT are consistent with our fluorescence spectra, Figs. 6 and 7. Namely, the quantum confinement of the DBT molecule in adsorption complex due to restricted in-plane vibrations of DBT in the nanocavity of the C300 MOF is consistent with the strong dispersive interactions of DBT molecule with hydrophobic benzene rings of the BTC linker as found by the DFT. Further, this study reports the coordinative bonding of the adsorbed DBT molecule to the Cu(II) as found by the DFT calculations. Our tentative explanation of bonding of one BT, DBT and 4,6-DMDBT molecule, on average, to one Cu_2O_8 unit (Table 1) is as follows. The structure of HKUST-1 contains three kinds of "cages" (Mason et al. 2014) that are commonly approximated as spheres of diameter 13.5, 11 and 5 Å. Only the surface of the largest "sphere" with diameter 13.5 Å contains the Cu(II) CUS (Senkovska et al. 2012; Mason et al. 2014). The surface areas of those spheres are: 143 $Å^2$ for the largest sphere with the CUS of dia. 13.5 Å, 95 $Å^2$ for the intermediate sphere of dia. 11 Å, and 19.6 $Å^2$ for the small sphere of dia. 5 Å. Therefore, the largest sphere with the Cu(II) CUS accounts, roughly, for one half of the total surface area, and contains one half of the total number of Cu(II) sites. Therefore, one molecule of BT, DBT or 4,6-DMDBT binds to each second Cu(II) site or, on average, to each Cu_2O_8 unit. The adsorbed amount of the smaller molecule thiophene corresponds to about 1.40 adsorbed molecules per one Cu_2O_8 unit, on average. The small thiophene molecule can apparently penetrate and bind to the adsorption sites within the smaller "spheres" where the larger BT, DBT and 4,6-DMDBT cannot penetrate and bind.

In summary, our combined in situ TPAD data on the adsorption capacity at variable temperature, the stoichiometry of the adsorption complexes at variable temperature, the wavelength-dependent fluorescence spectra of the adsorption complex and the DFT computations suggest that DBT in the adsorption complex with C300 MOF is located within the large hydrophilic cavity, weakly bound to the Cu(II) site at the Cu_2O_8 paddlewheel unit, and strongly dispersively stabilized by the side interactions with benzene rings of the BTC linker surrounding the Cu_2O_8 adsorption site.

7 Conclusions

Adsorption of aromatic sulfur compounds from model diesel with *n*-$C_{14}H_{30}$ as solvent onto C300 Basolite MOF containing Cu(II) CUS occurs via the non-reactive adsorption. The in situ temperature-programmed adsorption/desorption (TPAD) data show that BT adsorbs reversibly, while the larger 4,6-DMDBT adsorbs irreversibly in the temperature range 25–115 °C. Aromatic sulfur compounds BT, DBT and 4,6-DMDBT form the 1:1

stoichiometric adsorption complexes, with molar ratio (adsorbed molecule/Cu_2O_8 MOF unit) close to unity at 25 °C. Fluorescence spectroscopy confirms the quantum confinement of an adsorbed DBT molecule in the nanocavity of C300 MOF, and the interactions of adsorbed DBT with functional groups of the MOF are observed via the change of the relative intensities of the 0–0 and vibronically coupled 0–1 fluorescence transitions. Both the strong dispersive interactions of the aromatic rings of the aromatic sulfur compounds T and DBT with the BTC linker and weak electronic interactions of sulfur atom of aromatic sulfur compounds with Cu(II) CUS of C300 MOF contribute to the energy of bonding as determined by the DFT calculations.

Acknowledgments A.S. thanks Rutgers University for his Research Council Grant #202221. M.D. thanks the Ministry of National Education of Republic of Turkey for his graduate fellowship.

References

Achmann, S., Hagen, G., Hämmerle, M., Malkowsky, I.M., Kiener, C., Moos, R.: Sulfur removal from low-sulfur gasoline and diesel fuel by metal–organic frameworks. Chem. Eng. Technol. **33**(2), 275–280 (2010)

Alvarez-Valtierra, L., Yi, J.T., Pratt, D.W.: Lifetime broadening in the rotationally resolved electronic spectra of dibenzothiophene, 2,5-diphenylfuran, and 2,5-diphenyl-1,3,4-oxadiazole in the gas phase. Intersystem crossing dynamics in the statistical limit. J. Phys. Chem. A **113**(11), 2261–2267 (2009)

Bezverkhyy, I., Ortiz, G., Chaplais, G., Marichal, C., Weber, G., Bellat, J.P.: MIL-53(Al) under reflux in water: formation of gamma-AlO(OH) shell and H2BDC molecules intercalated into the pores. Microporous Mesoporous Mater. **183**, 156–161 (2014)

Blanco-Brieva, G., Campos-Martin, J.M., Al-Zahrani, S.M., Fierro, J.L.G.: Effectiveness of metal–organic frameworks for removal of refractory organo-sulfur compound present in liquid fuels. Fuel **90**(1), 190–197 (2011)

Bloch, E.D., Queen, W.L., Krishna, R., Zadrozny, J.M., Brown, C.M., Long, J.R.: Hydrocarbon separations in a metal-organic framework with open iron(II) coordination sites. Science **335**(6076), 1606–1610 (2012)

Bree, A., Zwarich, R.: Electronic spectra of dibenzothiophene. Spectrochim. Acta, Part A **27**(4), 621–630 (1971)

Burdett, J.J., Muller, A.M., Gosztola, D., Bardeen, C.J.: Excited state dynamics in solid and monomeric tetracene: the roles of superradiance and exciton fission. J. Chem. Phys. **133**(14) (2010)

Dai, J., McKee, M.L., Samokhvalov, A.: Adsorption of naphthalene and indole on F300 MOF in liquid phase by the complementary spectroscopic, kinetic and DFT studies. J. Porous Mat. (2014, accepted). doi:10.1007/s10934-014-9818-3

Del Riccio, J.L., Zhang, F.T., Lacey, A.R., Kable, S.H.: The electronic spectroscopy of 2,2 '-binaphthyl in solution, cryogenic matrix and supersonic jet. J. Phys. Chem. A **104**(32), 7442–7451 (2000)

Dhage, P., Samokhvalov, A., Repala, D., Duin, E.C., Bowman, M., Tatarchuk, B.J.: Copper-promoted ZnO/SiO2 regenerable sorbents for the room temperature removal of H2S from reformate gas streams. Ind. Eng. Chem. Res. **49**(18), 8388–8396 (2010)

Dhage, P., Samokhvalov, A., McKee, M.L., Duin, E.C., Tatarchuk, B.J.: Reactive adsorption of hydrogen sulfide by promoted sorbents Cu–ZnO/SiO2: active sites by experiment and simulation. Surf. Interface Anal. **45**(5), 865–872 (2013)

Farrusseng, D., Daniel, C.C., Gaudillère, C., Ravon, U., Schuurman, Y., Mirodatos, C., Dubbeldam, D., Frost, H., Snurr, R.Q.: Heats of adsorption for seven gases in three metal − organic frameworks: systematic comparison of experiment and simulation. Langmuir **25**(13), 7383–7388 (2009)

Gimeno-Fabra, M., Munn, A.S., Stevens, L.A., Drage, T.C., Grant, D.M., Kashtiban, R.J., Sloan, J., Lester, E., Walton, R.I.: Instant MOFs: continuous synthesis of metal–organic frameworks by rapid solvent mixing. Chem. Commun. **48**(86), 10642–10644 (2012)

Greathouse, J.A., Ockwig, N.W., Criscenti, L.J., Guilinger, T.R., Pohl, P., Allendorf, M.D.: Computational screening of metal–organic frameworks for large-molecule chemical sensing. PCCP **12**(39), 12621–12629 (2010)

Grimme, S., Ehrlich, S., Goerigk, L.: Effect of the damping function in dispersion corrected density functional theory. J. Comput. Chem. **32**(7), 1456–1465 (2011)

Ito, E., vanVeen, J.: On novel processes for removing sulphur from refinery streams. Catal. Today **116**, 446–460 (2006)

Jacob, J.: Sulfur Analogues of Polycyclic Aromatic Hydrocarbons (Thiaarenes). Cambridge (1990)

Jayaraman, A., Alptekin, G. O., Dubovik, M., Schaefer, M., Monroe, J., Bradley, K.: FUEL 212-desulfurization of liquid fuels by adsorption. Abstr. Pap. Am. Chem. Soc. **235** (2008)

Jee, B., Eisinger, K., Gul-E-Noor, F., Bertmer, M., Hartmann, M., Himsl, D., Pöppl, A.: Continuous wave and pulsed electron spin resonance spectroscopy of paramagnetic framework cupric ions in the Zn(II) doped porous coordination polymer Cu3 − xZnx(btc)2. J. Phys. Chem. C **114**(39), 16630–16639 (2010)

Kabešová, M., Boča, R., Melník, M., Valigura, D., Dunaj-Jurčo, M.: Bonding properties of thiocyanate groups in copper(II) and copper(I) complexes. Coord. Chem. Rev. **140**, 115–135 (1995)

Keskin, S., van Heest, T.M., Sholl, D.S.: Can metal–organic framework materials play a useful role in large-scale carbon dioxide separations? ChemSusChem **3**(8), 879–891 (2010)

Lakowicz, J.R.: Principles of Fluorescence Spectroscopy. Springer, Berlin (2006)

Liu, B., Zhu, Y., Liu, S., Mao, J.: Adsorption equilibrium of thiophenic sulfur compounds on the Cu-BTC metal–organic framework. J. Chem. Eng. Data **57**(4), 1326–1330 (2012)

Lukose, B., Supronowicz, B., Petkov, P., Frenzel, J., Kuc, A.B., Seifert, G., Vayssilov, G.N., Heine, T.: Structural properties of metal–organic frameworks within the density-functional based tight-binding method. Phys. Status Solidi B **249**(2), 335–342 (2012)

Marenich, A.V., Cramer, C.J., Truhlar, D.G.: Universal solvation model based on solute electron density and on a continuum model of the solvent defined by the bulk dielectric constant and atomic surface tensions. J. Phys. Chem. B **113**(18), 6378–6396 (2009)

Mason, J.A., Veenstra, M., Long, J.R.: Evaluating metal–organic frameworks for natural gas storage. Chem. Sci. **5**(1), 32–51 (2014)

McKinley, S.G., Angelici, R.J.: Deep desulfurization by selective adsorption of dibenzothiophenes on Ag+/SBA-15 and Ag+/SiO2. Chem. Commun. **20**, 2620–2621 (2003)

Nicholson, T.M., Bhatia, S.K.: Electrostatically mediated specific adsorption of small molecules in metallo-organic frameworks. J. Phys. Chem. B **110**(49), 24834–24836 (2006)

Petkov, P., Vayssilov, G.N., Liu, J., Shekhah, O., Wang, Y., Wöll, C., Heine, T.: Defects in MOFs: a thorough characterization. ChemPhysChem **13**(8), 2025–2029 (2012)

Prestipino, C., Regli, L., Vitillo, J.G., Bonino, F., Damin, A., Lamberti, C., Zecchina, A., Solari, P.L., Kongshaug, K.O.,

Bordiga, S.: Local structure of framework Cu(II) in HKUST-1 metallorganic framework: spectroscopic characterization upon activation and interaction with adsorbates. Chem. Mater. **18**(5), 1337–1346 (2006)

Robertson, J., Bandosz, T.J.: Photooxidation of dibenzothiophene on TiO2/hectorite thin films layered catalyst. J. Colloid Interface Sci. **299**, 125–135 (2006)

Ryzhikov, A., Bezverkhyy, I., Bellat, J.-P.: Reactive adsorption of thiophene on Ni/ZnO: role of hydrogen pretreatment and nature of the rate determining step. Appl. Catal. B Environ. **84**, 766–772 (2008)

Saha, D.P.D., Deng, S.G., Yang, Z.G.: Hydrogen adsorption on metal–organic framework (MOF-5) synthesized by DMF approach. J. Porous Mater. **16**(2), 141–149 (2009)

Samokhvalov, A.: Desulfurization of real and model liquid fuels using light: photocatalysis and photochemistry. Cat. Rev. Sci. Eng. **54**(3), 281–343 (2012)

Samokhvalov, A., Tatarchuk, B.J.: Review of experimental characterization of active sites and determination of molecular mechanisms of adsorption, desorption and regeneration of the deep and ultradeep desulfurization sorbents for liquid fuels. Cat. Rev. Sci. Eng. **52**(3), 381–410 (2010)

Samokhvalov, A., Duin, E.C., Nair, S., Bowman, M., Davis, Z., Tatarchuk, B.J.: Study of the surface chemical reactions of thiophene with Ag/titania by the complementary temperature-programmed electron spin resonance, temperature-programmed desorption, and X-ray photoelectron spectroscopy: adsorption, desorption, and sorbent regeneration mechanisms. J. Phys. Chem. C **114**, 4075–4085 (2010a)

Samokhvalov, A., Nair, S., Duin, E.C., Tatarchuk, B.J.: Surface characterization of Ag/titania adsorbents. Appl. Surf. Sci. **256**, 3647–3652 (2010b)

Samokhvalov, A., Duin, E.C., Nair, S., Tatarchuk, B.J.: An in situ temperature-programmed XPS study of the surface chemical reactions of thiophene with Ag/titania. Surf. Interface Anal. **42**(9), 1476–1482 (2010c)

Samokhvalov, A., Duin, E.C., Nair, S., Tatarchuk, B.J.: Adsorption and desorption of dibenzothiophene on Ag-titania studied by the complementary temperature-programmed XPS and ESR. Appl. Surf. Sci. **257**(8), 3226–3232 (2010d)

Senkovska, I., Barea, E., Navarro, J.A.R., Kaskel, S.: Adsorptive capturing and storing greenhouse gases such as sulfur hexafluoride and carbon tetrafluoride using metal–organic frameworks. Microporous Mesoporous Mater. **156**, 115–120 (2012)

Shan, G., Liu, H., Xing, J., Zhang, G., Wang, K.: Separation of polycyclic aromatic compounds from model gasoline by magnetic alumina sorbent based on pi-complexation. Ind. Eng. Chem. Res. **43**(3), 758–761 (2004)

Song, C.: Fuel processing for low-temperature and high-temperature fuel cells: challenges, and opportunities for sustainable development in the 21st century. Catal. Today **77**(1–2), 17–49 (2002)

Spanget-Larsen, J., Thulstrup, E.W.: The electronic transitions of dibenzothiophene: linear dichroism spectroscopy and quantum chemical calculations. J. Mol. Struct. **661–662**, 603–610 (2003)

Suezer, S.: XPS investigation of X-ray-induced reduction of metal ions. Appl. Spectrosc. **54**(11), 1716–1718 (2000)

Tozuka, Y., Tashiro, E., Yonemochi, E., Oguchi, T., Yamamoto, K.: Solid-state fluorescence study of naphthalene adsorption on porous material. J. Colloid Interface Sci. **248**, 239–243 (2002)

Vitillo, J.G., Regli, L., Chavan, S., Ricchiardi, G., Spoto, G., Dietzel, P.D.C., Bordiga, S., Zecchina, A.: Role of exposed metal sites in hydrogen storage in MOFs. J. Am. Chem. Soc. **130**, 8386–8396 (2008)

Xiang, S.-C., Zhang, Z., Zhao, C.-G., Hong, K., Zhao, X., Ding, D.-R., Xie, M.-H., Wu, C.-D., Das, M.C., Gill, R., Thomas, K.M., Chen, B.: Rationally tuned micropores within enantiopure metal–organic frameworks for highly selective separation of acetylene and ethylene. Nat. Commun. **2**, 204 (2011)

Xiao, Y.L., Yang, Q.Y., Liu, D.H., Zhong, C.L.: Computational design of metal–organic frameworks for aniline recovery from aqueous solution. CrystEngComm **15**(45), 9588–9595 (2013)